Journal of Korean Association of Crystal Growth
Vol. 6, No. 3 (1996) 431-438

Fe-rich precipitates in hot-pressed TiB_2

Kwang Bo Shim, Keun Ho Auh and Brian Ralph*
Ceramic Materials Research Institute, Hanyang University, Seoul 133-791, Korea
** Department of Materials Technology, Brunel University of West London, U.K.*

고온가압소결된 TiB_2에서의 철을 함유한 석출물

심광보, 오근호, Brian Ralph*
한양대학교 세라믹소재연구소, 서울, 133-791
** Department of Materials Technology, Brunel University of West London, U.K.*

Abstract Transmission electron microscopy has been used to investigate the microstructure of hot-pressed TiB_2. Thin foil specimens, prepared by conventional ion beam thinning, revealed many features which originated from the crystallographic anisotropy of hexagonal TiB_2. It was observed that in these specimens Fe-impurities are precipitated to form secondary Fe-rich phases at grain triple edges, in grain boundaries and sometimes in-grain. These Fe-rich precipitates were characterised by their coherence or semi-coherence to a favourably oriented grain at a grain triple edge or grain boundaries or to the matrix TiB_2 phase.

요 약 투과전자현미경을 이용하여 고온가압소결된 TiB_2의 미세구조를 분석하였다. Ion beam thinning에 의해서 준비된 박편시편은 육방정계 TiB_2의 결정학적 이방성에 기인한 특징을 보여주었다. 이들 시편에서 철분 불순물은 결정입 3중점, 결정입계 그리고 결정내에 2차상을 형성하는 것으로 확인되었고, 결정입 3중점이나 결정입계 혹은 matrix에서 유리하게 배향된 결정입에 coherence or semi-coherence한 특징을 나타내었다.

1. Introduction

Modern engineering ceramic materials need to retain their strength at high tem-

peratures during service and at the same time possess high oxidation, erosion and thermal-shock resistance. Titanium diboride (TiB_2) is one of the most suitable ceramics for such conditions due to its excellent properties ; a high melting point of 2980℃ [1], a low density of 4520 kgm^{-3} [2], an high hardness of 33 GPa [3], good electrical conductivity of $(7-11)\times10^6$ $W^{-1}m^{-1}$ [4], good thermal conductivity of (60-66) $Wm^{-1}K^{-1}$ [5,6], and good wettability by molten Al [7]. TiB_2 also resists oxidation to 1400℃ and is chemically inert to non-alkali molten salts and most corrosive environments [8].

Because of these excellent properties TiB_2 has been used in a number of applications : cutting tools, ballistic armour protection, rocket nozzles, components in evaporator crucibles for aluminizing paper and plastic film, solid cathodes in molten salt electrolysis, wear-resistant coatings and conductive layers [9,10]. However, its applicability as a high temperature structural ceramic has been still restricted due to mainly its brittleness, poor sinterability and anisotropic thermal expansion characteristics.

In general, the properties of TiB_2 are dependent on the fabrication route [11], the characteristics of the starting powder [12] and the density of the final compacts. In particular, the properties are very sensitive to the microstructure in particular the presence of impurities. The mechanical properties are very sensitive to additives [13,14]. Investigations of the high-temperature deformation of TiB_2 have shown strong effects of grain size and the presence of precipitates on the plastic yield behaviour [15,16].

A previous study [17] of the microstructure of this material shows non-uniformities in the chemical composition. These non-uniformities in micro-areas were related to the presence of additive elements such as Fe and W. They were present at grain boundaries and in their vicinity, forming diffuse layers. It was suggested that they were dissolved in the TiB_2 matrix replacing Ti, since no distinguishable change in the orientation between microareas enriched and free of them was found.

In the present work, we describe the behaviour of Fe impurity in the TiB_2 specimens as seen using transmission electron microscopy. Transmission electron microscopy combined with energy dispersive X-ray spectroscopy and electron diffraction analysis were used to characterize the microstructure and secondary phases which are sometimes found in association with dislocation arrays, and are also present in intra-grain and inter-grain areas. Some microscopic features associated with the secondary phases, such as a Moiré patterns and dislocations, are discussed. The detailed description of the TiB_2 samples studied are given in our previous paper.

2. Experimental results

2.1. Artifect

2.1.1. Ledge-type surface of thin foils

Samples prepared by conventional ion beam thinning exhibited many artifacts. Figure 1 shows a typical grain edge in a TiB_2 sample, revealing the ledge-type surface. This aspect is attributed to the crystallographic characteristics of hexagonal TiB_2, with its origin during ion beam thinning when {0001} close-packed layers tended to be revealed and therefore the resultant thin foils were not uniform in thickness.

2.1.2. Condensed argon

Figure 2 shows an example of a condensed argon gas bubble the identification of which was confirmed by energy dispersive X-ray spectroscopy. These bubbles are distributed with a size of 0.5~1.5 mm in length and 0.1~0.5 mm in width in the surface of the sample. The formation of the condensed argon bubbles are likely to be due to the diffusion of argon along the grain boundaries where it then accumulated and condensed during the ion-thinning process [18]. The occurrence of these argon bubbles was found on the grain boundaries, especially at grain triple edges, in foils thinned with a high angle ion-beam of about 30°.

2.2. Iron-rich precipitates

2.2.1. Triple edges of TiB_2

Figure 3 shows a typical example of a triangular shaped phase (dark contrast) at a TiB_2 grain edge of this sample. The corresponding energy dispersive X-ray spectrum of the dark phase at the grain edge reveals the presence of Fe and Ti but the spectrum of the surrounding grains reveals only Ti peaks. This result indicates that the phase in the central dark region is an Fe-rich phase.

Electron diffraction analysis revealed that the grain boundary between any two of the three surrounding grains (marked with A, B, and C) are high angle type and that the Fe-rich phase on the edge is coherent or semi-coherent with the one of

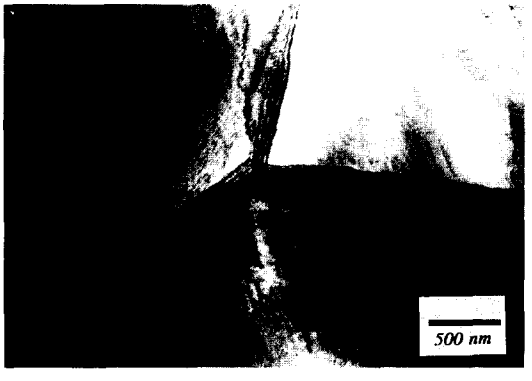

Fig. 1. TEM of the typical grain edge in TiB_2.

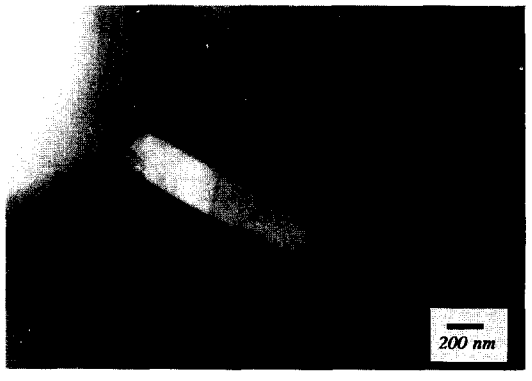

Fig. 2. TEM of a condensed argon gas bubble at a grain edge.

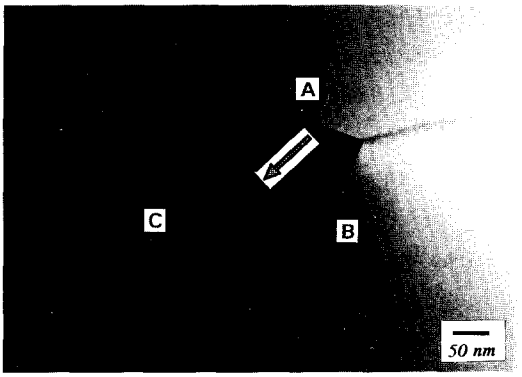

(a)

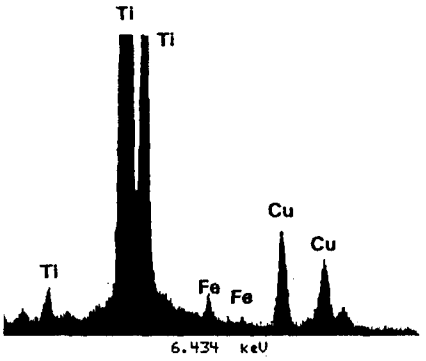

(b)

Fig. 3. TEM of the Fe-rich precipitates at the triple grain edge : (a) BF image and and (b) energy dispersive spectrum of the position indicated by an arrow in (a).

(a)

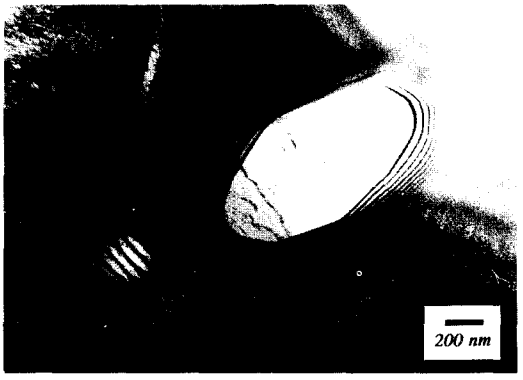

(b)

Fig. 4. TEM of the Fe-rich precipitate on the grain boundary.

the neighbouring grains at the edges.

2.2.2. Grain boundaries

The Fe-rich phase was observed at TiB_2 grain boundaries, as shown in Fig. 4 (a). Misfit dislocations at the boundary separating the matrix and the precipitate are seen. The precipitated phase is extremely thin and therefore only subtle contrast is visible on the side which overlaps the second grain. Figure 4 (b) is a micrograph of the same area as Fig. 4 (a) but with another orientation, revealing a hexagonal grid of dislocations on the interphase boundary. Energy dispersive spectra on this phase indicates that it is Fe-rich. Selected area electron diffraction analysis reveals that it is coherent or semi-coherent with the neighbouring TiB_2 grains having nearly the same interplanar spacings and the c lattice parameter is a little smaller because of the smaller atomic radius of Fe atoms (compared with Ti atoms [19]).

2.2.3. Interior of the TiB_2 grains

Fe-rich precipitates were also found in

the interior of the TiB_2 grains. Figure 5 shows a typical example of some isolated Fe-rich particles distributed within a TiB_2 grain. These Fe-rich crystalline precipitates were usually about 10~300 nm in size.

Figure 6 shows another example of Fe-rich precipitates in the interior of the TiB_2 grains. Electron diffraction analysis revealed that these Fe-rich phases were precipitated coherently with almost the same orientation as the surrounding TiB_2 matrix. However, the diffraction pattern from these Fe-rich precipitates loose their sharpness, showing diffuse Kikuchi lines (Fig. 7). This is thought to be due to the slight difference in the lattice parameter induced by the smaller atomic size of Fe.

The micrographs of Fig. 6 also shows that there are parallel lines in the Fe-rich precipitates. The presence of a Moiré pattern reinforced the explanation that these precipitates are associated with the smaller atomic size of Fe compared with Ti, because a Moiré pattern is generally formed by the lattice mismatch in the interface between the precipitates and the matrix [20].

Fig. 5. TEM of the Fe-rich particles distribution in a TiB_2 grain.

(a)

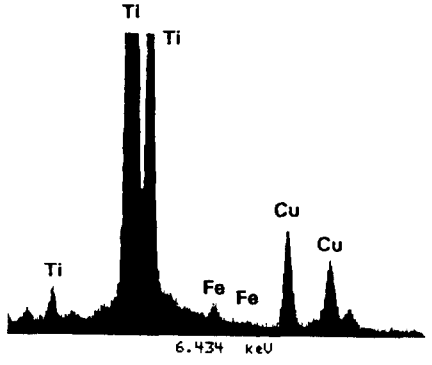

(b)

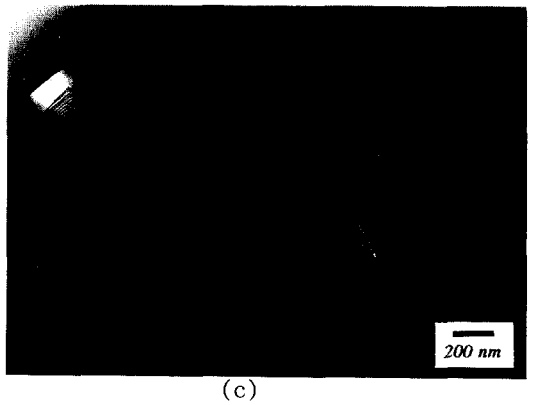

(c)

Fig. 6. TEM of the ingrain Fe-rich precipitates : (a) BF image, (b) EDS peaks of the precipitates and (c) BF image obtained from tilting of image (a) by 25.5°.

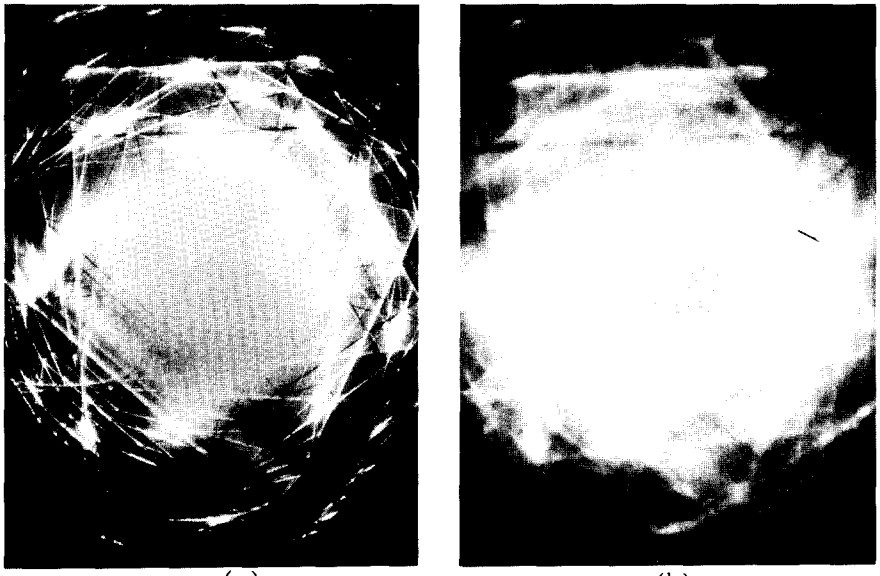

(a) (b)

Fig. 7. Selected area diffraction patterns of (a) the Fe-rich precipitates and (b) the surrounding TiB_2 matrix shown in Fig. 6, showing the diffuse Kikuchi lines in (b).

The parallel spacing of the Moiré lines is approximately 20 nm and neighbouring Fe-rich precipitates also showed the same orientation of the Moiré patterns.

The presence of dislocations near the Fe-rich precipitates also indicates the lattice mismatch in the boundary plane between the precipitates and the matrix. Figure 8 is a typical example showing that Fe-rich particles are associated with the presence of dislocations, where dislocation formation near the Fe-rich precipitates is seen. Figures 6 (a) and (c) also show the presence of interfacial dislocations on the Fe-rich precipitates.

The formation of these dislocations have as their origin the strains due to the lattice misfit between the Fe-rich phase and the surrounding TiB_2 matrix during the precipitation process or changes in thermal expansion coefficients. Most of the dislocations in Fig. 6 (c) are seen as initiated at the corners of the hexagonal Fe-rich precipitates, which are the most likely dislocation sources due to their high energy state.

The nature of these intra-grain precipitates was unknown, but it could be postulated that in the beginning it is only a stacking fault, because the basal plane is preferred for that kind of precipitation, and during the grain growth process it becomes more complex in nature.

3. Discussion

It was observed that the Fe-rich precipi-

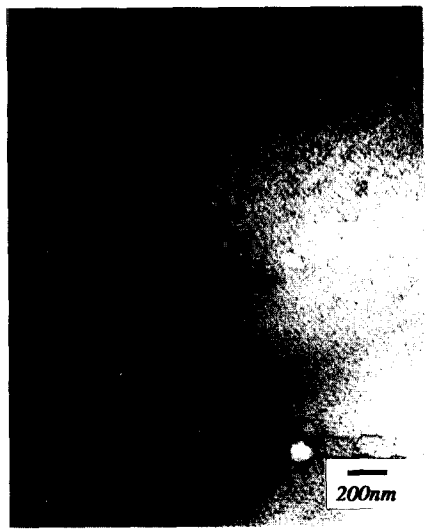

Fig. 8. TEM of the Fe-rich particle in a TiB_2 grain. The micrograph also shows the formation of dislocations.

tate at the triple edges of TiB_2 are coherent and/or semicoherent to one of the neighbouring grains. One possible explanation is that the Fe-rich phase had been in the liquid state during the hot-pressing process and has grown epitaxially on one of the three neighbouring grains. Although the exact crystallographic structure of the Fe-rich precipitates was impossible to determine by routine methods of electron diffraction because they are only a few hundred nanometres in size and quite thick as shown in Fig. 9, it is thought that they have a hexagonal structure with a chemical composition of $Fe_xTi_{1-x}B_2$.

The specimens investigated also showed that Fe segregates on grain boundaries and in the interior of grains, forming isolated Fe-rich precipitates. These precipitated phases were coherent or semi-coherent

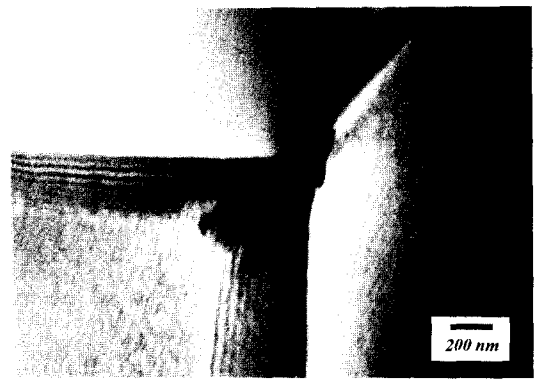

Fig. 9. TEM of the Fe-rich precipitates at a different orientation to Fig. 3 (a) showing the thickness of this precipitate.

with the surrounding TiB_2 grain (or matrix). It is thought that during the hot-pressing process, the Fe impurity dissolves to form a liquid phase at elevated temperatures and then the Fe-rich phases are precipitated in a crystalline form on cooling. The segregation of the Fe-rich phase is thought to be due to the partition of Fe when the amount of Fe exceeds the solubility limit in the TiB_2 matrix during the cooling process.

Fe-rich precipitated phases were observed mainly at grain edges rather than on grain boundaries. The reason for this is thought to be the low wetting angle of the liquid Fe-rich phase at the processing temperature. Therefore, the dihedral angles of the precipitates with the surrounding TiB_2 grains were such that grain-boundary penetration by the second-phase particles was uncommon.

W-rich diffuse layers near grain boundaries of a TiB_2 sample, which observed by

scanning electron microscopy and discussed in the previous study [17], were not observed by transmission electron microscopy. This was thought to be because the W-rich layers were not homogeneously distributed in the sample, as confirmed by scanning electron microscopy, and therefore the small area of observation by transmission electron microscopy did not detect the W-rich layer. Another possibility could also be that during the ion beam thinning the W-rich diffuse layers were removed preferentially.

References

[1] J.D. Latva, Metal Progress 82 (1962) 139.

[2] P.T. Shatter, Handbook of High-Temperature Materials : No.1 Materials Index (Plenum Press, New York, 1964) 55.

[3] P.W. Mott, Microindentation Hardness Testing (Butterworth's, London, 1956).

[4] A.D. McLeod, J.S. Haggerty and D. R. Sadoway, J. Am. Ceram. Soc. 67 (1984) 705.

[5] C.H. McMurtry, W.D.G. Boecker, S. G. Seshadri, J.S. Zanghi and J.E. Garnier, Am. Ceram. Soc. Bull. 66 (1987) 325.

[6] H. Itoh, S. Naka, T. Matsudaira and H. Hamamoto, J. Mater. Sci. 25 (1990) 533.

[7] R. Thompson, Progress in Boron Chemistry Vol. II, edited by R.J. Brotherton and H. Steinberg (Pergamon Press, Oxford, 1970) 173.

[8] P.C. Cobb, Material & Design 11 (1990) 156.

[9] J.B. Todd, J. Metals 33 (1981) 42.

[10] T.R. Shrout, A. Casciani, M. Mulvihill, D. Smith and W. Heubner, J. Mater. Sci. Letts. 9 (1990) 611.

[11] C. Mroz, Amer. Ceram. Soc. Bull. 72 (1993) 120.

[12] S. Baik and P.F. Becher, J. Am. Ceram. Soc. 70 (1987) 527.

[13] T. Watanabe and S. Kouno, Am. Ceram. Soc. Bull. 61 (1982) 970.

[14] E.S. Kang, C.W. Jang, C.H. Lee and C.H. Kim, J. Am. Ceram. Soc. **72** (1989) 1868.

[15] J.R. Ramberg, C.F. Wolfe and W.S. Williams, J. Am. Ceram. Soc. 68 (1985) C78-C79.

[16] J.R. Ramberg and W.S. Williams, J. Mater. Sci. 22 (1987) 1815.

[17] K.B. Shim, J. Kwiencinski, M.J. Edirisinghe and B. Ralph, Mater. Char. 31 (1993) 39.

[18] L. Michalowsky, H. Baumgartner and W. Ernst W, Ceram. Inter. 19 (1993) 77.

[19] W.A. Zdaniewski, J. Am. Ceram. Soc. 70 (1987) 793.

[20] R.E. Smallman, Modern Physical Metallurgy, 4th ed. (Butterworths, London, 1985) 249.